Radiation Physics and Chemistry xxx (xxxx) xxx–xxx

Contents lists available at ScienceDirect

Radiation Physics and Chemistry

journal homepage: www.elsevier.com/locate/radphyschem

Uncertainty propagation in activation cross section measurements

N. Otuka[a,b,*], B. Lalremruata[c], M.U. Khandaker[d], A.R. Usman[d,e], L.R.M. Punte[c]

[a] Nuclear Data Section, Division of Physical and Chemical Sciences, Department of Nuclear Sciences and Applications, International Atomic Energy Agency, A-1400 Wien, Austria
[b] Nishina Center for Accelerator-Based Science, RIKEN, Wako, Saitama 351-0198, Japan
[c] Department of Physics, Mizoram University, Tanhril, Aizawl 796004, India
[d] Department of Physics, University of Malaya, 50603 Kuala Lumpur, Malaysia
[e] Department of Physics, Umaru Musa Yar'adua University, Katsina, Nigeria

ARTICLE INFO

Keywords:
Activation cross section
Uncertainty
Uncertainty propagation
Covariance

ABSTRACT

The IAEA Nuclear Data Section (IAEA NDS) has emphasized the importance of archiving experimental nuclear data with detailed description of the uncertainties to provide reasonable evaluated (recommended) data sets with their uncertainties to end-users of nuclear data. In order to achieve this goal, the IAEA NDS is transferring relevant knowledge to experimentalists by instructing uncertainty propagation for their specific experiments. This article discusses uncertainty propagation based on detailed description of uncertainties in neutron- and charged-particle-induced activation cross sections measured in our studies.

1. Introduction

Activation of sample materials is a technique to determine nuclear reaction cross sections for radioisotope productions (activation cross sections) by measuring radiations from the radioactive products, and it has been widely applied to nuclear reactions with various projectiles (*e.g.*, neutron, charged-particle, photon) for many decades. Activation cross sections are basic nuclear data in a wide range of nuclear applications (*e.g.*, radioisotope production, reactor dosimetry, construction and decommission of nuclear facilities) as well as sciences (*e.g.*, nuclear astrophysics, cosmochemistry), and their experimental results have been utilized by end-users in various fields through compilation in the EXFOR Library (Otuka et al., 2014) and evaluation for development of general purpose nuclear reaction data libraries (*e.g.*, CENDL-3.1, Ge et al., 2011; ENDF/B-VII.1, Chadwick et al., 2011; JEFF-3.1.1, Santamarina et al., 2009; JENDL-4.0, Shibata et al., 2011; TENDL-2015, Koning and Rochman, 2012), activation data libraries (*e.g.*, EAF-2010, Sublet et al., 2010) as well as dosimetry data libraries (*e.g.*, IRDFF-1.05, Capote et al., 2012). The uncertainty accompanied with the activation cross section is essential in determination of reasonable margin contributing to both safety and economy in nuclear applications.

If several data points of the activation cross sections are involved in determination of the quantity of interest (*e.g.*, reaction rate obtained by folding of energy dependent activation cross sections by the spectrum characterizing the incident particle field), the correlation (covariance) among the data points has to also be considered to avoid overestimation or underestimation of the uncertainty in the quantity of interest. Due to this situation, modern evaluation tries to provide not only the best estimate of the cross section but also its uncertainty and covariance describing correlation among cross sections of the same reaction or even different reactions (cross correlation). In order to provide the uncertainty and covariance in addition to the best estimate of the cross section based on the experimental knowledge, data evaluators need detailed documentation of the uncertainties in each experiment. However evaluators often face difficulty due to lack of sufficient documentation of the experiment. At the worst case the evaluators cannot find any information on the uncertainty in the measured cross section, and it is also not rare to see a total uncertainty without its breakdown (*e.g.*, partial uncertainty due to counting statistics).

In order to improve the situation, the IAEA Nuclear Data Section (NDS) is encouraging experimentalists to perform appropriate uncertainty propagation and documentation in collaboration with external experts (Mannhart, 2013; Smith and Otuka, 2012; Schillebeeckx et al., 2012; Otuka et al., 2011, 2012; Otuka and Smith, 2014). However, we found that mere publications and presentations of guidelines are not sufficient to achieve our goal, and have thus recognized the importance to take more practical approaches relevant to designs of individual experiments.

* Corresponding author at: Nuclear Data Section, Division of Physical and Chemical Sciences, Department of Nuclear Sciences and Applications, International Atomic Energy Agency, A-1400 Wien, Austria.
E-mail addresses: n.otsuka@iaea.org (N. Otuka), marema_physics@mzu.edu.in (B. Lalremruata), mu_khandaker@um.edu.my (M.U. Khandaker).

http://dx.doi.org/10.1016/j.radphyschem.2017.01.013
Received 30 November 2016; Accepted 17 January 2017

In this article, we introduce two examples of our approach in real neutron- and charged-particle-induced activation cross section measurements performed in India and Japan, respectively, following a short summary on the basic concepts and uncertainty propagation formulae as well as a simple and hypothetical example demonstrating the importance of the uncertainty information for data evaluators.

2. Basic concepts and uncertainty propagation formulae

We consider various parameters required in cross section determinations (*e.g.*, number of counts, number of incident particles, number of atoms in the sample) as random variables x_k (k = 1, 2, ..) following a probability distribution function $p(x_1, x_2, ..)$ normalized as $\int_{-\infty}^{+\infty} \mathrm{d}\boldsymbol{x} p(x_1, x_2, \ldots) = 1$, where $\mathrm{d}\boldsymbol{x} = \mathrm{d}x_1\mathrm{d}x_2\ldots$. The mean value (best estimate) x_{k0}, covariance $\mathrm{Cov}(x_k, x_l)$, correlation coefficient $\mathrm{Cor}(x_k, x_l)$, variance $\mathrm{Var}(x_k)$, and standard deviation Δx_k are defined by

$$x_{k0} = \int \mathrm{d}\boldsymbol{x}\, x_k p(x_1, x_2, ..), \tag{1}$$

$$\mathrm{Cov}(x_k, x_l) = \int \mathrm{d}\boldsymbol{x}(x_k - x_{k0})(x_l - x_{l0})p(x_1, x_2, ..), \tag{2}$$

$$\mathrm{Cor}(x_k, x_l) = \mathrm{Cov}(x_k, x_l)/(\Delta x_k \Delta x_l), \tag{3}$$

$$\mathrm{Var}(x_k) = \int \mathrm{d}\boldsymbol{x}(x_k - x_{k0})^2 p(x_1, x_2, ..) = \mathrm{Cov}(x_k, x_k), \tag{4}$$

$$\Delta x_k = \sqrt{\mathrm{Var}(x_k)}, \tag{5}$$

respectively. By definition, $0 \le \mathrm{Cor}(x_k, x_l) \le 1$ and especially =1 when k=l. In nuclear data, one standard deviation of the parameter is usually treated as its *uncertainty*.[1] If x_1 is independent from the other parameters, we can decompose the probability distribution as

$$p(x_1, x_2, x_3, \ldots) = P(x_1)Q(x_2, x_3, \ldots), \tag{6}$$

and $\mathrm{Cov}(x_1, x_k) = 0$ ($k \neq 1$) according to the definition of the covariance.

If a set of quantities of interest $\{y_i\}$ are related to the parameters $\{x_k\}$ by $y_i = y_i(x_1, x_2, ..)$ and the relation can be linearized by expansion around the mean values of the parameters as

$$y_i = y_{i0} + \sum_k a_{ik}(x_k - x_{k0}) \tag{7}$$

with $y_{i0} = y_i(x_{10}, x_{20}, ..)$ and $a_{ik} = (\partial y_i/\partial x_k)_{x_k = x_{k0}}$ (sensitivity coefficient), the variance and covariance of x_k are propagated to those of y_i by

$$\mathrm{Var}(y_i) = \mathrm{Var}\left(\sum_k a_{ik}x_k\right) = \sum_k a_{ik}^2 \mathrm{Var}(x_k) + 2\sum_{k>l} a_{ik}\mathrm{Cov}(x_k, x_l)a_{il}, \tag{8}$$

$$\mathrm{Cov}(y_i, y_j) = \mathrm{Cov}\left(\sum_k a_{ik}x_k, \sum_l a_{jl}x_l\right) = \sum_k\sum_l a_{ik}\mathrm{Cov}(x_k, x_l)a_{jl}. \tag{9}$$

When y_i takes a multiplication form

$$y_i = \prod_k x_k^{g_{ik}} \tag{10}$$

with g_{ik} =+1, −1 or 0 (*e.g.*, $y_k = (x_1x_2x_3)/(x_4x_5x_6)$, $(x_1x_3)/(x_4x_5)$), the sensitivity coefficients are simplified to $a_{ik} = g_{ik}y_{i0}/x_{k0}$. If there is no correlation in $\{x_k\}$, Eq. (8) is simplified to

$$\mathrm{var}(y_i) = \sum_k g_{ik}^2 \mathrm{var}(x_k), \tag{11}$$

namely

$$(\Delta y_i/y_{i0})^2 = \sum_k g_{ik}^2(\Delta x_k/x_{k0})^2, \tag{12}$$

where the fractional variance $\mathrm{var}(\mu) = \mathrm{Var}(\mu)/\mu_0^2$ is introduced. This shows that the *quadratic sum* of the fractional (%) uncertainties in the parameters gives the fractional uncertainty in the quantity of interest. It is often forgotten that this quadratic sum formula is valid only when the quantity of interest is related with the parameters by Eq. (10).

When y_i is expressed in the form of Eq. (10) but correlation exists among $\{x_k\}$, Eqs. (8) and (9) are simplified to

$$\mathrm{var}(y_i) = \sum_k g_{ik}^2 \mathrm{var}(x_k) + 2\sum_{k>l} g_{ik}\mathrm{cov}(x_k, x_l)g_{il}, \tag{13}$$

$$\mathrm{cov}(y_i, y_j) = \sum_{k,l} g_{ik}\mathrm{cov}(x_k, x_l)g_{jl}, \tag{14}$$

where the relative covariance $\mathrm{cov}(\mu, \nu) = \mathrm{Cov}(\mu, \nu)/(\mu_0\nu_0)$ is introduced. Usually not all combinations of x_k and x_l have correlation but correlate each other within their n subsets such as $(x_1, x_2, \ldots, x_{M1})$, $(x_{M1+1}, \ldots, x_{M2})$, … . In such a case, the covariance terms in Eqs. (13) and (14) can be decomposed to

$$\sum_{k>l} g_{ik}\mathrm{cov}(x_k, x_l)g_{il} = \sum_{i=1}^{n}\sum_{k=M_{i-1}+1}^{M_i}\sum_{l=k+1}^{M_i} g_{ik}\mathrm{cov}(x_k, x_l)g_{il}, \tag{15}$$

$$\sum_{k,l} g_{ik}\mathrm{cov}(x_k, x_l)g_{jl} = \sum_{i=1}^{n}\sum_{k,l=M_{i-1}+1}^{M_i} g_{ik}\mathrm{cov}(x_k, x_l)g_{jl} \tag{16}$$

with $M_0 = 0$. For example, we expect that the number of counts C_i (always independent from other parameters), number of atoms in the samples per area n_i, and number of the incident particles Φ_i acting as six parameters $\{x_i\}$ (i=1,6) describing the cross sections σ_i=$C_i/(n_i\Phi_i)$ (i=1,2) has the following fractional covariances:

$$\begin{pmatrix} \mathrm{var}(C_1) & & & & & \\ 0 & \mathrm{var}(C_2) & & & & \\ 0 & 0 & \mathrm{var}(n_1) & & & \\ 0 & 0 & \mathrm{cov}(n_1, n_2) & \mathrm{var}(n_2) & & \\ 0 & 0 & 0 & 0 & 0 & \\ 0 & 0 & 0 & 0 & 0 & 0 \end{pmatrix} \tag{17}$$

if the uncertainty in Φ_i is negligible.

When y_i cannot be expressed by Eq. (10) and there is no correlation in parameters $\{x_k\}$, Eq. (8) can be rewritten as

$$(\Delta y_i/y_{i0})^2 = \sum_k s_{ik}^2(\Delta x_k/x_{k0})^2, \tag{18}$$

where

$$s_{ik} = (x_{k0}/y_{i0})(\partial y_i/\partial x_k)_{x_k = x_{k0}} = (x_{k0}/y_{i0})a_{ik} \tag{19}$$

is the relative sensitivity coefficient. Eq. (18) shows that we should distinguish the following two statements: "Uncertainty in y_i *due to* the uncertainty in x_k" (*i.e.*, $s_{ik}(\Delta x_k/x_{k0})$), and "Uncertainty *in* x_k" (*i.e.*, $\Delta x_k/x_{k0}$) though it is often not distinguished well in the literature.

A most typical situation creating correlation is seen when we assume two parameters to be equal. If $x_1 = x_2$ is assumed and they are independent from the rest of the parameters, we can decompose the probability distribution as

$$p(x_1, x_2, x_3, \ldots) = P(x_1)\delta(x_1 - x_2)Q(x_3, x_4, \ldots), \tag{20}$$

where $\delta(x)$ is the Dirac delta function.[2] By using

$$\int \mathrm{d}x_1\mathrm{d}x_2 P(x_1)\delta(x_1 - x_2)f(x_1, x_2) = \int \mathrm{d}x_1 P(x_1)f(x_1, x_1) = \int \mathrm{d}x_2 P(x_2)f(x_2, x_2)$$

for a given function $f(x_1, x_2)$, the variance and covariance of x_1 and x_2 are related by

$$\mathrm{Var}(x_1) = \mathrm{Var}(x_2) = \mathrm{Cov}(x_1, x_2), \tag{21}$$

[1] The uncertainty must be distinguished from the *error* which is the deviation of the best estimate from the true value. The true value is unknowable and therefore the error is also unknowable.

[2] $\delta(x) = 0$ for $x \neq 0$, and $\int_{-\infty}^{+\infty}\mathrm{d}x\,\delta(x) = 1$. From these properties, $\int_{-\infty}^{+\infty}\mathrm{d}x\,\delta(x - a)f(x) = f(a)$ for a given function $f(x)$.

and therefore $\mathrm{Cor}(x_1, x_2) = 1$ (fully correlated). On the other hand $\mathrm{Cor}(x_1, x_2) = 0$ (uncorrelated) when x_1 and x_2 are determined independently (*i.e.*, $p(x_1, x_2, x_3, \ldots) = p_1(x_1)p_2(x_2)Q(x_3, x_4, \ldots)$). A most typical uncorrelated parameter is the number of counts C for which $\Delta C = \sqrt{C}$ assuming that C is described by the Poisson distribution. The situation $0 < \mathrm{Cor}(x_1, x_2) < 1$ (partially correlated) occurs when x_1 and x_2 are determined not independently, but still x_2 is not automatically determined from x_1 (*i.e.*, $p(x_1, x_2, x_3, \ldots) = P(x_1, x_2)Q(x_3, x_4, \ldots)$). A typical situation creating this type of correlation is seen when x_1 and x_2 are on the same curve characterized by a set of parameters a, b, … such as $x_k = f(x_k; a, b, \ldots)$ (*e.g.*, two detection efficiencies obtained from the same efficiency curve characterized by parameters a, b, …). The correlation coefficients of two parameters uncorrelated, partially correlated, and fully correlated in their matrix expressions are therefore

$$\begin{pmatrix} 1 & 0 \\ 0 & 1 \end{pmatrix}, \quad \begin{pmatrix} 1 & r \\ r & 1 \end{pmatrix} \quad \text{and} \quad \begin{pmatrix} 1 & 1 \\ 1 & 1 \end{pmatrix}, \tag{22}$$

respectively ($0 < r < 1$).

Section B of Mannhart (2013) and Section II of Smith and Otuka (2012) provide good introductions to those who are interested in more details on the subjects discussed in this section.

3. Impact of experimental uncertainty on data evaluation

When sufficient experimental data points are available, the least squares method is a useful tool to determine the best estimate of the quantity in nuclear data evaluation. In order to demonstrate the importance of the detailed information on the experimental uncertainty for data evaluation, we discuss a simple and hypothetical example where an activation cross section σ is evaluated from two experimental data points by using the weighted mean, which is a special case of the least squares method (Appendix 2 of Mannhart, 2013). If we use the conventional weighted mean formula, the mean and variance of σ are

$$\begin{cases} \overline{\sigma} = \dfrac{V_2\sigma_1 + V_1\sigma_2}{V_1 + V_2}, \\ \mathrm{Var}(\sigma) = \dfrac{V_1V_2}{V_1 + V_2}, \end{cases} \tag{23}$$

where $V_i = \mathrm{Var}(\sigma_i)$. For a set of two experimental cross sections

$$\begin{cases} \sigma_1 = 100.0 \pm 5.0 \text{ mb} \\ \sigma_2 = 100.0 \pm 5.0 \text{ mb}. \end{cases} \tag{24}$$

Eq. (23) gives $\overline{\sigma} = 100.0 \pm 3.5$ mb. This result shows that the uncertainty was improved from 5.0 mb to 3.5 mb by repeating the experiment twice.

If σ_i is obtained from the number of counts C_i, number of incident particles irradiated the target Φ_i and number of atoms in the target per area n_i by

$$\sigma_i = C_i/(n_i\Phi_i), \tag{25}$$

$\Delta\sigma_i$ is then propagated from ΔC_i, $\Delta\Phi_i$ and Δn_i by

$$(\Delta\sigma_i/\sigma_i)^2 = (\Delta C_i/C_i)^2 + (\Delta n_i/n_i)^2 + (\Delta\Phi_i/\Phi_i)^2 \tag{26}$$

according to the quadratic sum formula of Eq. (12). The uncertainty obtained by the conventional weighted mean formula (3.5 mb) is correct as long as all three parameters C_i, Φ_i and n_i are determined in two experiments independently.

If there is a parameter not determined independently in two experiments, correlation exists between σ_1 and σ_2, and we have to use the off-diagonal weighted mean formula (Mannhart, 2013) instead of Eq. (23):

Table 1
Summary of results from two hypothetical experiments with their weighted mean.

	Exp.1	Exp.2	Remark
σ_i	100.0 mb	100.0 mb	
$\Delta\sigma_i/\sigma_i$	5%	5%	Total uncertainty
$\Delta C_i/C_i$	4%	4%	
$\Delta n_i/n_i$	3%		$n_1 = n_2$ assumed
$\Delta\Phi_i/\Phi_i$	(Negligible)	(Negligible)	
$\overline{\sigma}$	100 ± 3.5 mb		Conventional mean
	100 ± 4.1 mb		Off-diagonal mean

$$\begin{cases} \overline{\sigma} = \dfrac{(V_2 - V_{12})\sigma_1 + (V_1 - V_{12})\sigma_2}{V_1 + V_2 - 2V_{12}}, \\ \mathrm{var}(\sigma) = \dfrac{V_1V_2 - (V_{12})^2}{V_1 + V_2 - 2V_{12}}, \end{cases} \tag{27}$$

where $V_{12} = \mathrm{Cov}(\sigma_1, \sigma_2)$. Among six parameters, correlation may exist between Φ_1 and Φ_2, and n_1 and n_2, and therefore

$$V_{12} = \frac{\partial\sigma_1}{\partial\Phi_1}\mathrm{Cov}(\Phi_1, \Phi_2)\frac{\partial\sigma_2}{\partial\Phi_2} + \frac{\partial\sigma_1}{\partial n_1}\mathrm{Cov}(n_1, n_2)\frac{\partial\sigma_2}{\partial n_2} \tag{28}$$

according to Eq. (9). Note that $\mathrm{Cov}(C_1, C_2) = 0$ because the numbers of the counts from two experiments are always independent.

When it is difficult to obtain a certain amount of the target material (*e.g.*, minor actinide sample), two experiments performed at two laboratories sometimes share the same target material. If Φ_i was determined independently in two experiments (*e.g.*, $\mathrm{Cov}(\Phi_1, \Phi_2) = 0$), but n_i determined in one experiment is adopted in both experiments (*i.e.*, $n_1 = n_2 = n \pm \Delta n$), $\mathrm{Cov}(n_1, n_2) = (\Delta n)^2$ according to Eq. (21), and

$$V_{12} = (\sigma_1/n)(\Delta n)^2(\sigma_2/n). \tag{29}$$

For partial uncertainties of two measured cross sections summarized in Table 1, Eq. (27) gives 100.0 ± 4.1 mb instead of 100.0 ± 3.5 mb. This shows that the uncertainty of the weighted mean is less improved if we do not measure n_i twice independently.

This example demonstrates that the documentation of the data reduction equation (*e.g.*, Eq. (25)), partial uncertainties and their correlation properties (*e.g.*, Table 1) are necessary to estimate the uncertainty in the evaluated cross section properly.

4. Activation cross section measurements

In general, derivation of the activation cross section for the reaction of interest x is expressed by modifying Eq. (25) to

$$\sigma_x = \frac{C_x}{n_x\phi\epsilon_x I_x f_x} \tag{30}$$

where C_x, n_x, ϕ, ϵ_x and I_x are the number of counts, number of atoms in the target per area, number of incident particles per irradiation time, detection efficiency, and radiation intensity. The time factor f_x is defined by

$$f_x = (1 - e^{-\lambda_x t_i})e^{-\lambda_x t_{c,x}}(1 - e^{-\lambda_x t_{m,x}})/\lambda_x \tag{31}$$

with the irradiation time t_i, cooling time $t_{c,x}$, measurement time $t_{m,x}$, and decay constant λ_x.

In order to avoid direct measurement of ϕ, it is often determined by using a monitor (reference) reaction r for which

$$\sigma_r = \frac{C_r}{n_r\phi\epsilon_r I_r f_r} \tag{32}$$

with

$$f_r = (1 - e^{-\lambda_r t_i})e^{-\lambda_r t_{c,r}}(1 - e^{-\lambda_r t_{m,r}})/\lambda_r, \tag{33}$$

where the cross section σ_r (monitor cross section) is well established (*e.g.*, Carlson et al., 2009; Tárkányi et al., 2001), and we can rewrite Eq. (30) as

$$\sigma_x = \sigma_r \frac{C_x}{C_r}\frac{n_r}{n_x}\frac{\epsilon_r}{\epsilon_x}\frac{I_r}{I_x}\frac{f_r}{f_x}. \tag{34}$$

According to the quadratic sum formula (Eq. (12)), the uncertainty in σ_x is related with those in the parameters by

$$\left(\frac{\Delta\sigma_x}{\sigma_x}\right)^2 = \sum_q \left(\frac{\Delta q_x}{q_x}\right)^2 + \sum_q \left(\frac{\Delta q_r}{q_r}\right)^2 + \left(\frac{\Delta\sigma_r}{\sigma_r}\right)^2 \tag{35}$$

($q = C, n, \epsilon, I, f$) if all parameters appearing on the right-hand side of Eq. (34) are independent.

The following two subsections discuss two examples of activation cross section measurements (Punte et al., 2017; Lalremruata et al., 2017; Usman et al., 2017).

4.1. Neutron induced activation cross section measurement

The ^{70}Zn(n,γ)^{71m}Zn cross section was measured at the BARC Folded Tandem Ion Accelerator (FOTIA) Facility (Mumbai, India) by Mizoram University in collaboration with BARC and IAEA with the ^{197}Au(n,γ)^{198}Au reaction as a monitor reaction. A zinc foil enriched (72.4%) to ^{70}Zn was sandwiched by gold foils, and irradiated by neutrons produced by the ^{7}Li(p,n)^{7}Be reaction. The measured cross sections are still under analysis, and will be published separately (Punte et al., 2017; Lalremruata et al., 2017). Below, we discuss our determination of the uncertainty in the ^{70}Zn(n,γ)^{71m}Zn cross section due to the uncertainties in the detection efficiency, ^{197}Au(n,γ)^{198}Au monitor cross section and time factor.

4.1.1. Uncertainty in detection efficiency

In this experiment, a hyperpure germanium detector separated by 1 cm from the irradiated foil stack was used to determine C_x and C_r in Eq. (34). The detection efficiencies of the detector were measured by using eight γ-lines of a ^{152}Eu calibration source. The detection efficiency for the i-th γ-line (emission probability I_i, Martin, 2013) was determined by

$$\epsilon_i = \frac{C_i K_i}{A_0 e^{-\lambda t_c}(1 - e^{-\lambda t_m}) I_i}, \tag{36}$$

where C_i is the number of counts during the measuring time t_m, K_i is the correction factor for the coincidence summing effect, A_0 is the activity of the calibration source at the time of its manufacture, t_c is the time elapsed from the date of manufacturer to the start of counting, λ is the decay constant of ^{152}Eu. Fig. 1(a) shows the measured detection efficiencies.

We express the energy dependence of the detection efficiency by

$$\epsilon(E_\gamma) = \epsilon_0 \exp(-E_\gamma/E_0) + \epsilon_c, \tag{37}$$

where three parameters (ϵ_0, E_0 and ϵ_c) are determined by fitting this function to the measured detection efficiencies $\{\epsilon_i\}$ with their uncertainties propagated from $\Delta C_i = \sqrt{C_i}$ and ΔI_i determined by the ENSDF evaluator (Martin, 2013). Note that we do not have to propagate the uncertainties in the parameters commonly applied to all γ-lines (*e.g.*, ΔA_0, $\Delta\lambda$) because only the ratio of the detection efficiency ($\eta_{r,x} = \epsilon_r/\epsilon_x$) is required in our cross section determination. The fit parameters reproducing $\{\epsilon_i\}$ in Table 2 gives the detection efficiency curve $\epsilon(E_\gamma)$ in Fig. 1(a).

Applying Eq. (9) to Eq. (37), we can propagate the covariances of the three fit parameters to the two detection efficiencies at E_i and E_j on the curve by

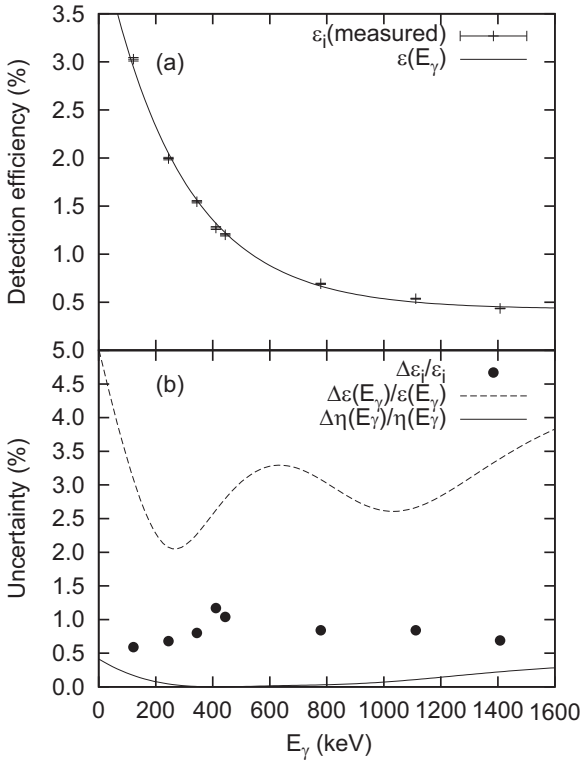

Fig. 1. (a) Detection efficiency curve $\epsilon(E)$ obtained from measured detection efficiencies for γ-lines of a ^{152}Eu calibration source ϵ_i (i = 1, 8). (b) The fractional uncertainties in the measured detection efficiencies ($\Delta\epsilon_i/\epsilon_i$), interpolated detection efficiency ($\Delta\epsilon(E_\gamma)/\epsilon(E_\gamma)$), and detection efficiency relative to the detection efficiency for the 411 keV γ-line of ^{197}Au ($\Delta\eta(E_\gamma)/\eta(E_\gamma)$), where $\eta(E_\gamma) = \epsilon(E_\gamma)/\epsilon(411\ \text{keV})$.

Table 2
The parameters of the detection efficiency curve $\epsilon(E_\gamma)$ reproducing the measured detection efficiencies $\{\epsilon_i\}$ with their uncertainties and correlation coefficients (×100).

Parameter	Value	Correlation coefficient		
ϵ_0	3.889 ± 0.208	100		
E_0 (keV)	279.541 ± 16.880	−84	100	
ϵ_c	0.428 ± 0.019	41	−69	100

$$\begin{aligned}\mathrm{Cov}(\epsilon(E_i), \epsilon(E_j)) = {} & e^{-\frac{E_i+E_j}{E_0}}(\Delta\epsilon_0)^2 + \frac{\epsilon_0^2 E_i E_j}{E_0^4} e^{-\frac{E_i+E_j}{E_0}}(\Delta E_0)^2 + (\Delta\epsilon_c)^2 \\ & + \epsilon_0 \frac{E_i + E_j}{E_0^2} e^{-\frac{E_i+E_j}{E_0}} \mathrm{Cov}(\epsilon_0, E_0) \\ & + \left(e^{-\frac{E_i}{E_0}} + e^{-\frac{E_j}{E_0}}\right)\mathrm{Cov}(\epsilon_0, \epsilon_c) \\ & + \frac{\epsilon_0}{E_0^2}\left(E_i e^{-\frac{E_i}{E_0}} + E_j e^{-\frac{E_j}{E_0}}\right)\mathrm{Cov}(E_0, \epsilon_c),\end{aligned} \tag{38}$$

which can be also used to obtain the uncertainty in the detection efficiency $(\Delta\epsilon_i)^2 = \mathrm{Cov}(\epsilon(E_i), \epsilon(E_i))$. Eq. (34) shows that we need only the ratio of the efficiencies $\eta_{r,x} = \epsilon_r/\epsilon_x$, which fractional uncertainty $\Delta\eta_{r,x}/\eta_{r,x}$ is propagated from $\mathrm{var}(\epsilon_x)$, $\mathrm{var}(\epsilon_r)$ and $\mathrm{cov}(\epsilon_r, \epsilon_x)$ by

$$\mathrm{var}(\eta_{r,x}) = \mathrm{var}(\epsilon_r) + \mathrm{var}(\epsilon_x) - 2\mathrm{cov}(\epsilon_r, \epsilon_x) \tag{39}$$

according to Eq. (13).

Fig. 1(b) compares the fractional uncertainty in the interpolated detection efficiency ratio $\Delta\eta(E_\gamma)/\eta(E_\gamma)$ with the fractional uncertainties in the measured detection efficiency $\Delta\epsilon_i/\epsilon_i$ and interpolated detection

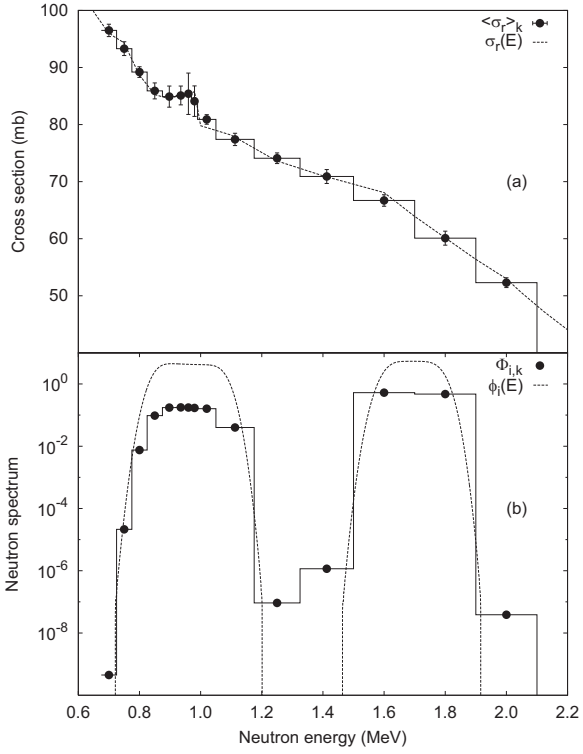

Fig. 2. (a) The point-wise ^{197}Au(n,γ)^{198}Au monitor cross section $\sigma_r(E)$ in the IAEA Neutron Cross-Section Standards (Carlson et al., 2009) and its group-wise expression $\langle\sigma_r\rangle_k$. (b) The ^{7}Li(p,n$_0$)^{7}Be point-wise neutron flux energy spectrum $\phi_i(E)$ calculated by EPEN (Pachuau et al., 2017a, 2017b) and its group-wise expression $\Phi_{i,k}$ (i=1,2; k=1–11 and k=12–15 for i = 1 and 2, respectively).

efficiency $\Delta\epsilon(E_\gamma)/\epsilon(E_\gamma)$. This figure shows that the uncertainty in the interpolated detection efficiency is larger than those in the measured detection efficiencies, however the uncertainty is drastically reduced if we use the ratio of the interpolated detection efficiencies due to the third term of Eq. (39). The uncertainty in $\eta_{r,x}$ approaches zero especially when the γ-line of the reaction product is very close to the γ-line of the monitor reaction product ^{198}Au (411 keV). Actually the γ-line of the reaction product ^{71m}Zn (386 keV) is in this situation, and we finally obtained its detection efficiency ratio with very low uncertainty $\Delta\eta_{r,x}/\eta_{r,x}$ = 0.257%.

4.1.2. Uncertainty in monitor cross section

The ^{197}Au(n,γ)^{198}Au cross section in the IAEA Neutron Cross-Section Standards (Carlson et al., 2009, Fig. 2(a)) was adopted as the monitor cross section in this experiment. Because the ^{7}Li(p,n$_0$)^{7}Be incident neutron beam is not monoenergetic but has energy spread (E_n=0.96 ± 0.15 and 1.69 ± 0.15 MeV, see Fig. 2(b)), the point-wise monitor cross section in the IAEA Neutron Cross-Section Standards $\sigma_r(E)$ was folded by the neutron flux energy spectrum $\phi_i(E)$ ($\int_0^\infty dE\phi_i(E) = 1$; i=1 and 2 are for E_n= 0.96 and 1.69 MeV) calculated by a newly developed code EPEN (Pachuau et al., 2017a, 2017b):

$$\bar{\sigma}_{r,i} = \int dE\phi_i(E)\sigma_r(E). \tag{40}$$

The IAEA Neutron Cross-Section Standards provide the covariance information of $\sigma_r(E)$ for its group-wise cross section expression:

$$\langle\sigma_r\rangle_k = \left(\int_{E_{k,\min}}^{E_{k,\max}} dE\sigma_r(E)\right) \Big/ (E_{k,\max} - E_{k,\min}), \tag{41}$$

where $E_{k,\min}$ and $E_{k,\max}$ are the lower and upper boundaries of the k-th energy group. Similarly, we also introduce the group-wise neutron flux energy spectrum $\Phi_{i,k}$ by

$$\Phi_{i,k} = \int_{E_{k,\min}}^{E_{k,\max}} dE\phi_i(E) \tag{42}$$

which satisfies $\sum_k \Phi_{i,k} = 1$. These group-wise quantities are shown in Fig. 2 and Table 3, where k=1–11 and 12–15 are for the E_n = 0.96 ± 0.15 and 1.69 ± 0.15 MeV neutrons, respectively.

By using $\langle\sigma_r\rangle_k$ and $\Phi_{i,k}$, Eq. (40) is discretized to

$$\bar{\sigma}_{r,i} = \sum_k \Phi_{i,k}\langle\sigma_r\rangle_k. \tag{43}$$

Then the uncertainty and covariance in the IAEA Neutron Cross-Section Standards are propagated to $\bar{\sigma}_{r,i}$ by

$$\mathrm{Var}(\bar{\sigma}_{r,i}) = \sum_k \Phi_{i,k}^2 \mathrm{Var}(\langle\sigma_r\rangle_k) + 2\sum_{k<l} \Phi_{i,k}\mathrm{Cov}(\langle\sigma_r\rangle_k, \langle\sigma_r\rangle_l)\Phi_{i,l} \tag{44}$$

$$\mathrm{Cov}(\bar{\sigma}_{r,i}, \bar{\sigma}_{r,j}) = \sum_{k,l} \Phi_{i,k}\mathrm{Cov}(\langle\sigma_r\rangle_k, \langle\sigma_r\rangle_l)\Phi_{j,l} \tag{45}$$

according to Eqs. (8) and (9). Table 4 summarizes the spectrum averaged monitor cross section $\bar{\sigma}_{r,i}$ with its uncertainty and correlation coefficient.

Table 3
Group-wise neutron flux energy spectrum $\Phi_{i,k}$ as well as IAEA Neutron Cross-Section Standards (Carlson et al., 2009) group-wise cross section $\langle\sigma_r\rangle_k$ with its uncertainty and correlation coefficients (×100). k=1–11 and 12–15 are corresponding to the E_n= 0.96 and 1.69 MeV neutrons, respectively. The groups are defined by the following boundary energies: 0.675, 0.725, 0.775, 0.825, 0.875, 0.920, 0.950, 0.970, 0.990, 1.050, 1.175, 1.325, 1.500, 1.700, 1.900 and 2.100 MeV (cf. Fig. 2).

i	k	$\Phi_{i,k}$	$\langle\sigma_r\rangle_k$ (mb)	Correlation coefficient														
1	1	5.730E−10	96.45 ± 1.09	100														
	2	2.746E−05	93.22 ± 1.21	44	100													
	3	9.641E−03	89.10 ± 0.93	34	52	100												
	4	1.231E−01	85.87 ± 1.40	20	29	33	100											
	5	1.975E−01	84.91 ± 1.85	13	12	13	11	100										
	6	1.314E−01	85.10 ± 1.64	7	13	25	15	9	100									
	7	8.559E−02	85.36 ± 3.62	3	4	6	10	3	6	100								
	8	8.430E−02	84.09 ± 2.67	8	6	7	6	44	5	2	100							
	9	2.438E−01	80.81 ± 0.84	19	15	25	25	20	38	11	12	100						
	10	1.247E−01	77.33 ± 1.08	16	14	14	13	13	21	7	9	45	100					
	11	2.884E−07	73.98 ± 0.93	17	16	18	13	12	6	3	12	28	41	100				
2	12	1.018E−06	70.84 ± 1.22	12	10	12	9	8	11	7	7	16	17	39	100			
	13	5.295E−01	66.60 ± 1.00	14	12	14	11	11	11	4	8	19	15	23	35	100		
	14	4.705E−01	59.99 ± 1.22	10	9	11	8	9	8	7	7	14	11	13	15	37	100	
	15	3.030E−08	52.12 ± 0.85	12	11	12	9	10	9	4	8	16	13	15	12	25	38	100

Table 4
Spectrum averaged monitor cross section, its uncertainty and correlation coefficients (×100).

i	E_n (MeV)	$\bar{\sigma}_{r,i}$ (mb)	Correlation coefficient	
1	0.96	82.77 ± 0.86	100	
2	1.69	64.09 ± 0.92	7	100

4.1.3. Uncertainty in time factor

We measured the γ-lines of the reaction product ^{71m}Zn and monitor product ^{198}Au simultaneously, and therefore we can set $t_{c,x} = t_{c,r} = t_c$ and $t_{m,x} = t_{m,r} = t_m$ in Eqs. (31) and (33). Then these time factors contain five sources of uncertainties t_i, t_c, t_m, λ_r and λ_x. Among them, the uncertainties in t_i, t_c and t_m are considered as negligible in this experimental work, and therefore only the uncertainties in λ_r and λ_x have to be propagated. Some researchers include the uncertainty in the decay constants in the quadrature sum formula such as $(\Delta\sigma_x/\sigma_x)^2 = \cdots + (\Delta\lambda_x/\lambda_x)^2 + (\Delta\lambda_r/\lambda_r)^2 + \cdots$, but this is wrong because the decay constant is related with the cross section through the exponential function. The correct way is to calculate the uncertainties in the time factors f_x and f_r, and propagate them to the uncertainty in σ_x by $(\Delta\sigma/\sigma)^2 = \cdots + (\Delta f_x/f_x)^2 + (\Delta f_r/f_r)^2 + \cdots$. The uncertainties in the time factors should be propagated from the uncertainties in the decay constants by

$$(\Delta f/f)^2 = s_{f\lambda}^2(\Delta\lambda/\lambda)^2 \tag{46}$$

($f = f_x$ or f_r, and $\lambda = \lambda_x$ or λ_r) with the relative sensitivity $s_{f\lambda}$

$$s_{f\lambda} = \frac{\lambda}{f}\frac{\partial f}{\partial \lambda} = \left(\frac{\lambda t_i e^{-\lambda t_i}}{1-e^{-\lambda t_i}} - \lambda t_c + \frac{\lambda t_m e^{-\lambda t_m}}{1-e^{-\lambda t_m}} - 1\right). \tag{47}$$

The uncertainty in the decay constant $\Delta\lambda = (\ln 2\Delta T_{1/2})/T_{1/2}^2$ can be obtained from $\Delta T_{1/2}$ in the ENSDF Library. This equation shows that the sensitivity depends not only on λ but also on t_i, t_c and t_m even though the uncertainties in the latter three parameters are treated as negligible. The obtained $\Delta f/f$ for ^{71m}Zn and ^{198}Au are given in Table 5. Note that the relative sensitivity coefficient $s_{f\lambda} \sim 1$ when λt_i, λt_c and $\lambda t_m \to 0$.

4.1.4. Covariance of measured cross sections

Table 5 summarizes the uncertainties in various parameters to obtain the ^{70}Zn(n,γ)^{71m}Zn cross section. We use Eq. (34) for these parameters except for replacement of ϵ_x and ϵ_r with η, and therefore we can use the quadratic sum formula to obtain the total uncertainty. The 22 parameters in Table 5 form the 13 subsets $C_{Zn,1}$, $C_{Zn,2}$, $C_{Au,1}$, $C_{Au,2}$, $(a_{Zn,1}, a_{Zn,2})$, $(n_{Zn,1}, n_{Zn,2})$, $(n_{Au,1}, n_{Au,2})$, $(I_{Zn,1}, I_{Zn,2})$, $(I_{Au,1}, I_{Au,2})$, $(f_{Zn,1}, f_{Zn,2})$, $(f_{Au,1}, f_{Au,2})$, (η_1, η_2), $(\sigma_{Au,1}, \sigma_{Au,2})$. From the uncertainties and correlation coefficients summarized in Table 5, we can construct the fractional variance and covariance by adding the matrices of 13 subsets according to Eqs. (14) and (16):

$$\begin{aligned}
&\begin{pmatrix} 7.809^2 & 0 \\ 0 & 0 \end{pmatrix} + \begin{pmatrix} 0 & 0 \\ 0 & 5.988^2 \end{pmatrix} + \begin{pmatrix} 3.247^2 & 0 \\ 0 & 0 \end{pmatrix} + \begin{pmatrix} 0 & 0 \\ 0 & 2.471^2 \end{pmatrix} \\
&+ \begin{pmatrix} 1.381^2 & 1.381^2 \\ 1.381^2 & 1.381^2 \end{pmatrix} + \begin{pmatrix} 0.115^2 & 0 \\ 0 & 0.088^2 \end{pmatrix} + \begin{pmatrix} 0.099^2 & 0 \\ 0 & 0.097^2 \end{pmatrix} \\
&+ \begin{pmatrix} 2.298^2 & 2.298^2 \\ 2.298^2 & 2.298^2 \end{pmatrix} + \begin{pmatrix} 0.063^2 & 0.063^2 \\ 0.063^2 & 0.063^2 \end{pmatrix} \\
&+ \begin{pmatrix} 0.177^2 & 0.177 \times 0.273 \\ 0.177 \times 0.273 & 0.273^2 \end{pmatrix} \\
&+ \begin{pmatrix} 0.027^2 & 0.027 \times 0.015 \\ 0.027 \times 0.015 & 0.015^2 \end{pmatrix} + \begin{pmatrix} 0.257^2 & 0.257^2 \\ 0.257^2 & 0.257^2 \end{pmatrix} \\
&+ \begin{pmatrix} 1.043^2 & 1.043 \times 1.433 \times 0.07 \\ 1.043 \times 1.433 \times 0.07 & 1.433^2 \end{pmatrix} = \begin{pmatrix} 79.924 & 7.317 \\ 7.317 & 51.377 \end{pmatrix} \\
&= \begin{pmatrix} 8.94^2 & 8.94 \times 7.17 \times 0.12 \\ 8.94 \times 7.17 \times 0.12 & 7.17^2 \end{pmatrix}.
\end{aligned} \tag{48}$$

The last term shows that the total uncertainties in the cross sections are 8.94% and 7.17% at 0.96 and 1.69 MeV, respectively, and also the correlation coefficient between the two cross sections is 0.12.

4.2. Charged-particle induced activation measurement

A series of measurements have been performed for deuteron and alpha induced activation cross sections at the AVF cyclotron of the RIKEN Nishina Center for Accelerator-Based Science (Wako, Japan) by the University of Malaya in collaboration with RIKEN and IAEA (Usman et al., 2017; Khandaker et al., 2013a,b, 2014a–c, 2015a,b; Usman et al., 2016a,b). In these experiments, a number of metallic foils are stacked and irradiated simultaneously (stacked foil activation). The energy of the incident particle decreases as the incident particle moves to the downstream side of the stack, and finally it stops at a foil of the stack. In our experiments, the front foil (*i.e.*, the foil placed at the most upstream side of the stack) directly irradiated by the incident particle extracted from the cyclotron is a titanium foil which serves as a monitor foil to determine ϕ using monitor reactions such as ^{nat}Ti(d,x)^{48}V and ^{nat}Ti(α,x)^{51}Cr which cross sections are well established (*e.g.*, Tárkányi et al., 2001), and we treat the obtained ϕ as a constant through the whole foil stack. Activities of the irradiated foils were measured by a coaxial hyperpure germanium detector at various distances between the irradiated foil and detector.

4.2.1. Uncertainty propagation of the γ-intensity

At an earlier stage of these experiments (Khandaker et al., 2013a,b, 2014a,b, 2015a), we set the following *assumption* in our uncertainty propagation:

- 5% for the uncertainty in ϕ (originated from the uncertainties in σ_r, C_r, n_r, ϵ_r, I_r),
- 4% for the uncertainty in ϵ_x,
- 1% for uncertainties in n_x and I_x,
- uncertainties in other parameters (except for C_x) are negligible.

Table 5
Fractional uncertainties (%) in various parameters to obtain the ^{70}Zn(n,γ)^{71m}Zn cross section.

i	E_n (MeV)	Δσ (%)											
		C_{Zn}	C_{Au}	a_{Zn}	n_{Zn}	n_{Au}	I_{Zn}	I_{Au}	f_{Zn}	f_{Au}	η	σ_{Au}	Total
1	0.96	7.809	3.247	1.381	0.115	0.099	2.298	0.063	0.177	0.027	0.257	1.043	8.94
2	1.69	5.988	2.471	1.381	0.088	0.097	2.298	0.063	0.273	0.015	0.257	1.433	7.17
Correlation		0	0	1	0	0	1	1	1	1	1	0.07	0.12

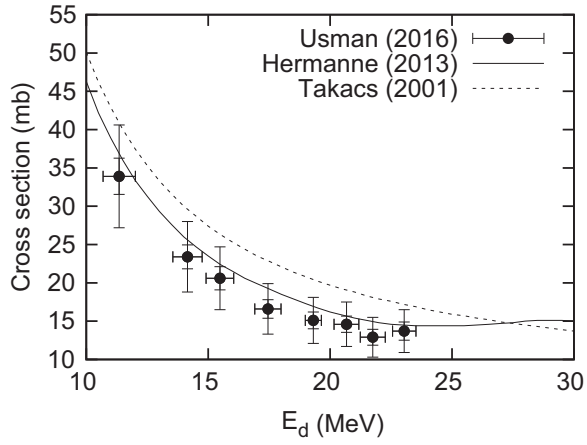

Fig. 3. Excitation functions of ^{nat}Ni(d,x)^{61}Cu determined by detection of the 656 keV γ-line (Usman et al., 2016a) with two error bars (shorter error bars obtained with $\Delta I_\gamma/I_\gamma = 1\%$, and longer error bars obtained with $\Delta I_\gamma/I_\gamma = 18.519\%$, Zuber and Singh, 2015). The data sets recommended by Hermanne et al. (2013) and Takàcs et al. (2001) are also plotted.

However we realized that the uncertainty in I_x strongly depends on the selected γ-line (from ~0.001% to ~10%). The source of I_x adopted in our experiments (ENSDF Library, Bhat, 1992) also provides ΔI_x, and we started to propagate the uncertainty determined by the ENSDF evaluators (Usman et al., 2016a,b, 2017) instead of 1% uncertainty in our recent works. Fig. 3 shows an impact due to adoption of the $\Delta I_x/I_x$ determined by the ENSDF evaluators. In this figure, the ^{nat}Ni(d,x)^{61}Cu cross section measured by us (Usman et al., 2016a) by counting the 656 keV γ-line ($I_x = 0.108$ γ/decay, Zuber and Singh, 2015) is compared with those recommended by Hermanne et al. (2013) and Takàcs et al. (2001). The shorter and longer error bars are respectively corresponding to adoption of our conventional uncertainty $\Delta I_x/I_x = 1\%$ and of the uncertainty evaluated by the ENSDF evaluators ($\Delta I_x/I_x = 18.519\%$, Zuber and Singh, 2015). This figure shows that the cross sections measured by us become more consistent with the cross section recommended by Hermanne et al. by adoption of ΔI_x determined by the ENSDF evaluators.

4.2.2. Deviation from quadratic sum formula

Sometimes we have to combine the numbers of counts for two γ-lines to obtain the cross section of interest. Such an example is seen in our determination of the ^{nat}Ti(α,x)^{44g}Sc cross section (Usman et al., 2017). Fig. 4 shows the decay scheme of ^{44g}Sc and ^{44m}Sc. The ^{nat}Ti(α,x)^{44m}Sc cross section $\sigma_{m,i}$ was simply determined from the number of counts for 271 keV γ-line $C_{271,i}$ ($I_{271} = 0.867$ γ/decay, Chen et al., 2011):

$$\sigma_{m,i} = \frac{C_{271,i}}{n\phi\epsilon_{271}I_{271}f_m}, \tag{49}$$

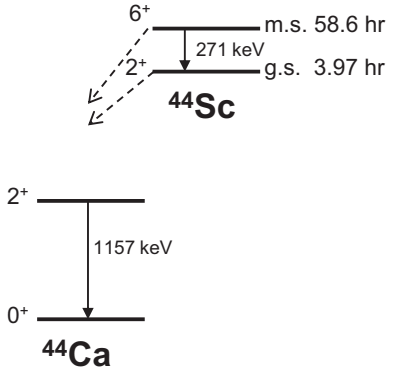

Fig. 4. Decay scheme of ^{44g}Sc (3.97 h) and ^{44m}Sc (58.6 h).

(i=1,4 for $E_\alpha = 51$, 48, 44 and 39 MeV) with ϕ determined by measurement of the 320 keV γ-line from ^{nat}Ti(α,x)^{51}Cr monitor reaction:

$$\phi = \frac{1}{\sigma_r}\frac{C_r}{n\epsilon_r I_r f_r}. \tag{50}$$

Note that titanium foils with the same thickness are used for determination of both σ_x and ϕ, and therefore we set $n_x = n_r = n$. Eq. (49) has a functional form of Eq. (10), and therefore we can apply the quadratic sum formula (Eq. (12)) to all parameters of this equation.

The situation is complicated for the ^{nat}Ti(α,x)^{44g}Sc cross section $\sigma_{g,i}$, for which the 1157 keV γ-line is only strong one available for observation of the ground state. However this γ-line is emitted by both ground and metastable states ($I_{1157,g} = 0.999$ γ/decay and $I_{1157,m} = 0.0120$ γ/decay), and these states are connected by the isomeric transition ($b_{IT} = 0.988$) (Chen et al., 2011). The number of counts for 1157 keV γ-line $C_{1157,i}$ is decomposed to three components:

$$C_{1157,i} = n\phi\epsilon_{1157}\left[\sigma_{g,i}\, I_{1157,g} f_g + \sigma_{m,i}\, I_{1157,m} f_m + \sigma_{m,i}\, b_{IT}\, I_{1157,g}\frac{\lambda_m\lambda_g}{\lambda_m - \lambda_g}\left(\frac{f_g}{\lambda_g} - \frac{f_m}{\lambda_m}\right)\right], \tag{51}$$

where the first term is for emission from the directly produced ground state, the second term is for emission from the metastable state, and the third term is for emission from the ground state originated from the isomeric transition of the metastable state. By solving this equation in terms of $\sigma_{g,i}$ and combining it with Eq. (49), we obtain $\sigma_{g,i}$ as a function of $C_{271,i}$ and $C_{1157,i}$:

$$\sigma_{g,i} = \frac{1}{n\phi I_{1157,g} f_g}\left[\frac{C_{1157,i}}{\epsilon_{1157}} - \frac{C_{271,i}}{\epsilon_{271}}\frac{I_{1157,m}}{I_{271}} - \frac{C_{271,i}}{\epsilon_{271}}\frac{b_{IT}I_{1157,g}}{I_{271}f_m}\frac{\lambda_m\lambda_g}{\lambda_m - \lambda_g}\left(\frac{f_g}{\lambda_g} - \frac{f_m}{\lambda_m}\right)\right]\alpha(\beta - \gamma - \delta). \tag{52}$$

This equation shows that we have to propagate uncertainties in the 10 parameters $\{x_k\} = \{n, \phi, \epsilon_{1157}, \epsilon_{271}, C_{1157,i}, C_{271,i}, I_{1157,g}, I_{1157,m}, I_{271}, b_{IT}\}$ summarized in Table 6 to the uncertainty in $\sigma_{g,i}$. Assuming that these parameters at a given energy are independent of each other, we can use Eq. (18) to propagate the uncertainty in x_k to $\sigma_{g,i}$, where the explicit forms of the relative sensitivity coefficients s_{ik} are

$$(n/\sigma_{g,i})(\partial\sigma_{g,i}/\partial n) = 1,\ (\phi/\sigma_{g,i})(\partial\sigma_{g,i}/\partial\phi) = 1,$$
$$(\epsilon_{1157}/\sigma_{g,i})(\partial\sigma_{g,i}/\partial\epsilon_{1157}) = -\alpha\beta/\sigma_{g,i},\ (\epsilon_{271}/\sigma_{g,i})(\partial\sigma_{g,i}/\partial\epsilon_{271}) = (\alpha/\sigma_{g,i})(\gamma + \delta),$$
$$(C_{1157,i}/\sigma_{g,i})(\partial\sigma_{g,i}/\partial C_{1157,i}) = (\alpha/\sigma_{g,i})\beta,$$
$$(C_{271,i}/\sigma_{g,i})(\partial\sigma_{g,i}/\partial C_{271,i}) = -(\alpha/\sigma_{g,i})(\gamma + \delta),$$
$$(I_{1157,g}/\sigma_{g,i})(\partial\sigma_{g,i}/\partial I_{1157,g}) = -(\alpha/\sigma_{g,i})(\beta - \gamma),$$
$$(I_{1157,m}/\sigma_{g,i})(\partial\sigma_{g,i}/\partial I_{1157,m}) = -(\alpha/\sigma_{g,i})\gamma,$$
$$(I_{271}/\sigma_{g,i})(\partial\sigma_{g,i}/\partial I_{271}) = (\alpha/\sigma_{g,i})(\gamma + \delta),\ (b_{IT}/\sigma_{g,i})(\partial\sigma_{g,i}/\partial b_{IT}) = -(\alpha/\sigma_{g,i})\delta.$$

Table 6 shows that the quadratic sum formula is valid (*i.e.*, $s_{ik} = 1$) for two parameters n and ϕ as it is obvious from Eq. (52). We also can see that the parameters for the 1157 keV γ-line are slightly more sensitive (~1.2) than those in the quadratic sum formula, while those for the 271 keV γ-line have little influence (~0.2) on the total uncertainty. If we wrongly apply the quadratic sum formula to all parameters, the total uncertainty of $\sigma_{g,i}$ is ~7.81% at all α energies, which is almost determined by the four parameters having the largest fractional uncertainties (n, ϕ, ϵ_{1157} and ϵ_{271}). Correct uncertainty propagation gives the smaller total uncertainty due to the small sensitivity of ϵ_{271} except for one data point at 39 MeV where the correct uncertainty propagation gives a larger uncertainty than the use

Table 6
Parameters (x_k) for determination of ^{nat}Ti(α,x)^{44g}Sc at four α energies $\sigma_{g,i}$ (i=1,4) (Usman et al., 2017) with their fractional (%) uncertainties $\Delta x_k/x_k$ and relative sensitivity coefficients s_{ik}. The parenthesized energies in MeV give the incident α energies. The italicized fractional uncertainties are empirically determined values. The symbol ~ shows that the s_{ik} value slightly depends on the incident α energy. "Neg." means that the uncertainty in the parameter is considered as negligible.

Parameter	x_k	$\Delta x_k/x_k$ (%)	s_{ik}
n	5.88E−8 atoms/mb	*2*	1.0
ϕ	5.45E+11 α/sec	*5*	1.0
ϵ_{1157}	0.001204	*4*	~−1.2
ϵ_{271}	0.004273	*4*	~0.2
$C_{1157,i}$	9053 (51 MeV)	1.05	1.2
	8251 (48 MeV)	1.10	1.2
	5405 (44 MeV)	1.36	1.2
	1473 (39 MeV)	2.61	1.3
$C_{271,i}$	7245 (51 MeV)	1.17	−0.2
	6977 (48 MeV)	1.20	−0.2
	4786 (44 MeV)	1.45	−0.2
	1498 (39 MeV)	2.58	−0.3
$I_{1157,g}$	0.999 γ/decay	0.40	~1.2
$I_{1157,m}$	0.012 γ/decay	5.83	0.0
I_{271}	0.867 γ/decay	0.35	~0.2
b_{IT}	0.988	0.07	~−0.2
t_i	7200 s	Neg.	
t_m	200 s	Neg.	
t_c	15 240 s (51 MeV)	Neg.	
	14 880 s (48 MeV)	Neg.	
	14 520 s (44 MeV)	Neg.	
	14 220 s (39 MeV)	Neg.	
λ_g	4.85E−05 1/s	Neg.	
λ_m	3.29E−06 1/s	Neg.	

of the quadratic sum formula because of the large uncertainty in $C_{1157,i}$. Table 7 summarizes the total and partial uncertainties in $\sigma_{g,i}$ at four α energies.

4.2.3. Correlation between cross sections at two energies

So far we considered all parameters to obtain the ^{44m}Sc and ^{44g}Sc production cross sections are independent at a given α energy. However correlation of some parameters must be considered if we study the relation of cross sections at the four α energies. For example, uncertainty propagation of ^{44m}Sc production cross sections obtained by Eq. (49) at the four α energies involves 20 parameters which are $C_{271,i}$, $n_i(=n)$, $\phi_i(=\phi)$, $\epsilon_{271,i}(=\epsilon_{271})$, $I_{271,i}(=I_{271})$ with i=1,4. They are propagated to the variance and covariance of the cross section by

$$\mathrm{var}(\sigma_{m,i}) = \mathrm{var} = (C_{271,i}) + \mathrm{var}(n_i) + \mathrm{var}(\phi_i) + \mathrm{var}(\epsilon_{271,i}) + \mathrm{var}(I_{271,i}) = \mathrm{var}(C_{271,i}) + \mathrm{var}(n) + \mathrm{var}(\phi) + \mathrm{var}(\epsilon_{271}) + \mathrm{var}(I_{271}), \quad (53)$$

$$\mathrm{cov}(\sigma_{m,i}, \sigma_{m,j}) = \mathrm{cov}(n_i, n_j) + \mathrm{cov}(\phi_i, \phi_j) + \mathrm{cov}(\epsilon_{271,i}, \epsilon_{271,j}) + \mathrm{cov}(I_{271,i}, I_{271,j}) = \mathrm{var}(n) + \mathrm{var}(\phi) + \mathrm{var}(\epsilon_{271}) + \mathrm{var}(I_{271}) = 2^2 + 5^2 + 4^2 + 0.35^2 \sim 45(\%^2) \quad (i \neq j) \quad (54)$$

according to Eqs. (13) and (14). By using $\Delta\sigma_{m,i}/\sigma_{m,i} = \sqrt{\mathrm{var}(\sigma_{m,i})}$ in Table 7, these fractional variance and covariance are summarized as

$$\begin{pmatrix} 6.82^2 & & & \\ 45 & 6.82^2 & & \\ 45 & 45 & 6.87^2 & \\ 45 & 45 & 45 & 7.20^2 \end{pmatrix}, \quad (55)$$

and the corresponding correlation coefficients are

$$\begin{pmatrix} 1 & & & \\ 45/6.82/6.82 & 1 & & \\ 45/6.82/6.87 & 45/6.82/6.87 & 1 & \\ 45/6.82/7.20 & 45/6.82/7.20 & 45/6.87/7.20 & 1 \end{pmatrix}. \quad (56)$$

The above example shows that the construction of the covariance matrix is relatively easy when only uncorrelated and fully correlated uncertainties in the parameters are propagated by the quadratic sum formula, and especially the fractional values of the fully correlated uncertainties are the same at all data points.

A possible improvement in the error propagation discussed above is to consider the correlation between the detection efficiencies of the 271 keV γ-line from the reaction product ^{44m}Sc (ϵ_{271}) and of the 320 keV γ-line from the monitor product ^{51}Cr (ϵ_{320}). If we propagate the uncertainty in ϵ_{320} explicitly by considering its correlation with ϵ_{271} instead of inclusion of the uncertainty in ε_{320} in the assumed constant uncertainty in ϕ (5%), there might be a major change in the contribution of the uncertainties in these detection efficiencies to the total uncertainty because their γ-lines are relatively close. The full publication of the experiment (Usman et al., 2017) will also report the ^{nat}Ti(α,x)^{51}Cr cross sections for which the uncertainty in the detection efficiency should disappear because the same reaction is also used as a monitor reaction to determine ϕ, and ϵ_x and ϵ_r of Eq. (34) cancel each other. See also the discussion on Fig. 1(b) of Section 4.1.1 for the treatment of the correlation between detection efficiencies.

5. Conclusions

We have discussed examples of uncertainty propagation for neutron and charged-particle activation cross section measurements in detail following introduction of basic concepts and uncertainty propagation formulae as well as importance of detailed documentation of the uncertainty. Our two examples show that we need not only the total uncertainty but also partial uncertainties and their correlation properties of each data point to obtain the covariance information of the activation cross sections.

The actual data reduction equation of our neutron activation cross sections has correction factors to take into account various effects (*e.g.*, contribution of ^{7}Li(p,n$_1$)^{7}Be low energy (parasitic) neutron capture, capture of neutron scattered by the sample and surrounding materials, absorption of γ-rays by the sample materials before detection). These correction factors are omitted in Eq. (34), and we did not evaluate their uncertainties. It is not realistic to evaluate the uncertainties of all parameters included in the data reduction equation, and the propagation formulae show the importance to identify the parameters which have major contributions to the uncertainty propagation, and to estimate their uncertainties and correlation properties carefully. Some web sites maintained by the IAEA NDS (*e.g.*, Verpelli and

Table 7
^{nat}Ti(α,x)^{44g,m}Sc cross sections and their uncertainties (Usman et al., 2017). Partial uncertainties are also given for ^{44g}Sc production cross sections.

i	E_α (MeV)	$\sigma_{g,i}$ (mb)	$\Delta\sigma_{g,i}$ (%)										$\sigma_{m,i}$ (mb)	$\Delta\sigma_{m,i}$ (%)
			Total	n	ϕ	ϵ_{1157}	ϵ_{271}	$C_{1157,i}$	$C_{271,i}$	$I_{1157,g}$	$I_{1157,m}$	I_{271}	b_{IT}		Total
1	51	7.03	7.36	2.00	5.00	4.77	0.77	1.25	0.23	0.48	0.02	0.07	0.01	13.72	6.82
2	48	6.24	7.40	2.00	5.00	4.81	0.81	1.32	0.24	0.48	0.02	0.07	0.01	13.20	6.82
3	44	3.99	7.50	2.00	5.00	4.84	0.84	1.65	0.30	0.48	0.02	0.07	0.01	9.05	6.87
4	39	1.04	8.13	2.00	5.00	4.98	0.98	3.25	0.64	0.50	0.03	0.09	0.02	2.83	7.20

Abriola, 2011; Zerkin and Trkov, 2008) provide friendly interfaces for extraction of the uncertainties in various nuclear data originally compiled in complicated formats.

Acknowledgment

The work described in this paper would not have been possible without IAEA Member States contributions. One of us (N.O.) would like to thank D.L. Smith and W. Mannhart for their advice in dealing with covariance data, and also H. Haba and V. Semkova for their advices on experimental aspects of activation cross section determination.

References

Bhat, M.R., 1992. In: Qaim, S.M. (Ed.), Proceedings of the International Conference on Nuclear Data for Science and Technology, Jülich, Germany, 13–17 May 1991. Springer-Verlag, Berlin, Germany, 1992, p. 817.
Capote, R., Zolotarev, K.I., Pronyaev, V.G., Trkov, A., 2012. J. ASTM Int. 9, (JAI104119).
Carlson, A.D., Pronyaev, V.G., Smith, D.L., Larson, N.M., Chen, Zhenpeng, Hale, G.M., Hambsch, F.-J., Gai, E.V., Oh, Soo-Youl, Badikov, S.A., Kawano, T., Hofmann, H.M., Vonach, H., Tagesen, S., 2009. Nucl. Data Sheets 110, 3215.
Chadwick, M.B., Herman, M., Obložinský, P., Dunn, M.E., Danon, Y., Kahler, A.C., Smith, D.L., Pritychenko, B., Arbanas, G., Arcilla, R., Brewer, R., Brown, D.A., Capote, R., Carlson, A.D., Cho, Y.S., Derrien, H., Guber, K., Hale, G.M., Hoblit, S., Holloway, S., Johnson, T.D., Kawano, T., Kiedrowski, B.C., Kim, H., Kunieda, S., Larson, N.M., Leal, L., Lestone, J.P., Little, R.C., McCutchan, E.A., MacFarlane, R.E., MacInnes, M., Mattoon, C.M., McKnight, R.D., Mughabghab, S.F., Nobre, G.P.A., Palmiotti, G., Palumbo, A., Pigni, M.T., Pronyaev, V.G., Sayer, R.O., Sonzogni, A.A., Summers, N.C., Talou, P., Thompson, I.J., Trkov, A., Vogt, R.L., van der Marck, S.C., Wallner, A., White, M.C., Wiarda, D., Young, P.G., 2011. Nucl. Data Sheets 112, 2887.
Chen, J., Singh, B., Cameron, J.A., 2011. Nucl. Data Sheets 112, 2357.
Ge, Z.G., Zhuang, Y.X., Liu, T.J., Zhang, J.S., Wu, H.C., Zhao, Z.X., Xia, H.H., 2011. J. Korean Phys. Soc. 59, 1052.
Hermanne, A., Takàcs, S., Adam-Rebeles, R., Tàrkànyi, F., Takàcs, M.P., 2013. Nucl. Instrum. Methods Phys. Res. B 299, 8, (EXFOR D4282).
Khandaker, M.U., Haba, H., Kanaya, J., Otuka, N., 2013a. Nucl. Instrum. Methods Phys. Res. B 296, 14, (EXFOR E2404).
Khandaker, M.U., Haba, H., Kanaya, J., Otuka, N., 2013b. Nucl. Instrum. Methods Phys. Res. B 316, 33, (EXFOR E2439).
Khandaker, M.U., Haba, H., Otuka, N., Usman, A.R., 2014a. Nucl. Instrum. Methods Phys. Res. B 335, 8, (EXFOR E2457).
Khandaker, M.U., Haba, H., Kanaya, J., Otuka, N., Kassim, H.A., 2014b. Nucl. Data Sheets 119, 252, (EXFOR E2462).
Khandaker, M.U., Haba, H., Murakami, M., Otuka, N., Kassim, H.A., 2014c. J. Radioanal. Nucl. Chem. 302, 759, (EXFOR E2467).
Khandaker, M.U., Haba, H., Murakami, M., Otuka, N., 2015a. Nucl. Instrum. Methods Phys. Res. B 346, 8, (EXFOR E2473).
Khandaker, M.U., Haba, H., Murakami, M., Otuka, N., Kassim, H.A., 2015b. Nucl. Instrum. Methods Phys. Res. B 362, 151, (EXFOR E2485).
Koning, A.J., Rochman, D., 2012. Nucl. Data Sheets 113, 2841.
Lalremruata, B., Punte, L.R.M., Otuka, N., Pachuau, R., Iwamoto, Y., Suryanarayana, S. V., Nayak, B.K., Satheesh, B., Thanga, H.H., Danu, L.S., Desai, V.V., Hlondo, L.R., Ganesan, S., Saxena, A., 2017. INDC(IND)-0049, International Atomic Energy Agency, in preparation.
Mannhart, W., 2013. INDC(NDS)-0588 Rev., International Atomic Energy Agency.
Martin, M.J., 2013. Nucl. Data Sheets 114, 1497.
Otuka, N., Smith, D.L., 2014. Nucl. Data Sheets 120, 281.
Otuka, N., Borella, A., Kopecky, S., Lampoudis, C., Schillebeeckx, P., 2011. J. Korean Phys. Soc. 59, 1314.
Otuka, N., Capote, R., Kopecky, S., Plompen, A.J.M., Pronyaev, V.G., Schillebeeckx, P., Smith, D.L., 2012. In: EPJ Web of Conference, vol. 27, p. 00007.
Otuka, N., Dupont, E., Semkova, V., Pritychenko, B., Blokhin, A.I., Aikawa, M., Babykina, S., Bossant, M., Chen, G., Dunaeva, S., Forrest, R.A., Fukahori, T., Furutachi, N., Ganesan, S., Ge, Z., Gritzay, O.O., Herman, M., Hlavač, S., Katõ, K., Lalremruata, B., Lee, Y.O., Makinaga, A., Matsumoto, K., Mikhaylyukova, M., Pikulina, G., Pronyaev, V.G., Saxena, A., Schwerer, O., Simakov, S.P., Soppera, N., Suzuki, R., Takćs, S., Tao, X., Taova, S., Tárkányi, F., Varlamov, V.V., Wang, J., Yang, S.C., Zerkin, V., Zhuang, Y., 2014. Nucl. Data Sheets 120, 272.
Pachuau, R., Lalremruata, B., Otuka, N., Hlondo, L.R., Punte, L.R.M., Thanga, H.H., 2017b. EPJ Web of Conferences. ND2016: International Conference on Nuclear Data for Science and Technology, 11–16 September 2016, Bruge, Belgium, in preparation.
Pachuau, R., Lalremruata, B., Otuka, N., Hlondo, L.R., Punte, L.R.M., Thanga, H.H., 2017a. Nucl. Sci. Eng., (in press).
Punte, L.R.M., Lalremruata, B., Otuka, N., Suryanarayana, S.V., Iwamoto, Y., Pachuau, R., Satheesh, B., Thanga, H.H., Danu, L.S., Desai, V.V., Hlondo, L.R., Kailas, S., Ganesan, S., Nayak, B.K., Saxena, A., 2017. Phys. Rev. C, (in press).
Santamarina, A., Bernard, D., Blaise, P., Coste, M., Courcelle, A., Huynh, T.D., Jouanne, C., Leconte, P., Litaize, O., Mengelle, S., Noguère, G., Ruggiéri, J.-M., Sérot, O., Tommasi, J., Vaglio, C., Vidal, J.-F., 2009. JEFF Report 22. OECD NEA Data Bank.
Schillebeeckx, P., Becker, B., Danon, Y., Guber, K., Harada, H., Heyse, J., Junghans, A.R., Kopecky, S., Massimi, C., Moxon, M.C., Otuka, N., Sirakov, I., Volev, K., 2012. Nucl. Data Sheets 113, 3054.
Shibata, K., Iwamoto, O., Nakagawa, T., Iwamoto, N., Ichihara, A., Kunieda, S., Chiba, S., Furutaka, K., Otuka, N., Ohsawa, T., Murata, T., Matsunobu, H., Zukeran, A., Kamada, S., Katakura, J., 2011. J. Nucl. Sci. Technol. 48, 1.
Smith, D.L., Otuka, N., 2012. Nucl. Data Sheets 113, 3006.
Sublet, J.-Ch., Packer, L.W., Kopecky, J., Forrest, R.A., Koning, A.J., Rochman, D.A., 2010. CCFE-R(10)05. Culham Centre for Fusion Energy.
Takàcs, S., Szelecsenyi, F., Tàrkànyi, F., Sonck, M., Hermanne, A., Shubin, Yu., Dityuk, A., Mustafa, M.G., Zhuang, Youxiang, 2001. Nucl. Instrum. Methods Phys. Res. B 174, 235, (EXFOR D4081).
Tárkányi, F., Takács, S., Gul, K., Hermanne, A., Mustafa, M.G., Nortier, M., Obložinský, P., Qaim, S.M., Scholten, B., Shubin, Yu.N., Zhuang Youxiang, 2001. IAEA-TECDOC 1211. International Atomic Energy Agency, p. 49.
Usman, A.R., Khandaker, M.U., Haba, H., Murakami, M., Otuka, N., 2016a. Nucl. Instrum. Methods Phys. Res. B 368, 112, (EXFOR E2492).
Usman, A.R., Khandaker, M.U., Haba, H., Otuka, N., Murakami, M., Komori, Y., 2016b. Appl. Radiat. Isot. 114, 104, (EXFOR E2511).
Usman, A.R., Khandaker, M.U., Haba, H., Otuka, N., Murakami, M., 2017. Submitted to Nucl. Instrum. Methods Phys. Res. B.
Verpelli, M., Abriola, D., 2011. J. Korean Phys. Soc. 59, 1322.
Zerkin, V., Trkov, A., 2008. In: Bersillon, O., Gunsing, F., Bauge, E., Jacqmin, R., Leray, S. (Eds.), Proceedings of the International Conference on Nuclear Data for Science and Technology, Nice, France, 22–27 April 2007. EDP Sciences, Les Ulis, France, p. 769.
Zuber, K., Singh, B., 2015. Nucl. Data Sheets 125, 1.